BİNGÖL UNIVERSITY

Turkish Journal of Nature and Science

e-ISSN: 2149-6366
www.dergipark.gov.tr/tdfd

Research Article

Volume 15, Issue 1, Page 202-212, 2026

Received: 20.01.2026
Accepted: 13.03.2026
Published: 30.03.2026

DOI: https://doi.org/10.46810/tdfd.1867831

# Tuning Cisplatin–Graphene Interactions: The Impact of Dopant Identity and Concentration

**Cahit ÖREK**[1*]

[1] Kastamonu Univ, Res & Applicat Ctr, TR37150 Kastamonu, Turkey

**Corresponding author: cahitorek@gmail.com*

## Abstract

Cisplatin remains a cornerstone of cancer therapy, yet its efficacy is compromised by severe toxicity and off-target uptake, driving the search for targeted delivery systems such as graphene-based nanocarriers. Despite the promise of heteroatom doping to enhance drug loading, a detailed mechanistic understanding of how dopant identity and concentration alter the delicate balance of noncovalent forces is lacking. This study aims to elucidate the atomic-level drivers of cisplatin physisorption on boron- and nitrogen-doped graphene nano-fragments. Using dispersion-corrected density functional theory (PBE-D3(BJ)) coupled with energy decomposition analysis via DFT-SAPT, this study reveals that moderate doping significantly strengthens adsorption. Specifically, boron dopants enhance binding through electrostatic complementarity, whereas nitrogen dopants primarily increase polarization and induction effects. However, a key finding is that higher dopant loadings lead to an "electronic smoothing" of the surface potential, unexpectedly weakening the binding affinity. These results suggest a practical "doping window" of 5–8% as an optimal design strategy for engineering graphene carriers with strong yet controlled drug retention.

## Keywords

Cisplatin,
Graphene nanocarriers,
Heteroatom doping,
Drug delivery,
Noncovalent interactions

BİNGÖL ÜNİVERSİTESİ

Türk Doğa ve Fen Dergisi

e-ISSN: 2149-6366
www.dergipark.gov.tr/tdfd

Araştırma Makalesi

Cilt 15, Sayı 1, Sayfa 202-212, 2026

Alınış: 20.01.2026
Kabul: 13.03.2026
Basım: 30.03.2026

DOI: https://doi.org/10.46810/tdfd.1867831

# Sisplatin-Grafen Etkileşiminin Modülasyonu: Katkı Türü ve Konsantrasyonun Etkisi

**Cahit ÖREK**[1*]

[1] Kastamonu Üniversitesi, Araştırma ve Uygulama Merkezi, TR37150, Kastamonu, Türkiye

**Sorumlu yazar: cahitorek@gmail.com*

## Özet

Sisplatin, kanser tedavisinin temel taşlarından biri olma özelliğini korumakla birlikte; etkinliği, ciddi toksisite ve hedef dışı etki sorunları nedeniyle gölgelenmektedir. Bu durum, grafen tabanlı nanotaşıyıcılar gibi hedeflendirilmiş iletim sistemlerine yönelik arayışı tetiklemektedir. Heteroatom katkılama işlemi grafenin ilaç taşınım potansiyelini artırmasına rağmen; katkı maddesinin kimliği ve konsantrasyonunun, kovalent olmayan kuvvetlerin dengesini ne yönde değiştirdiği henüz tam olarak anlaşılamamıştır. Bu çalışma, sisplatinin bor ve azot katkılı grafen nano-parçacıkları ile etkileşimini atomik düzeyde yönlendiren etkileri aydınlatmayı amaçlamaktadır. DFT-SAPT analizleri ile desteklenen ve dispersiyon düzeltmeli yoğunluk fonksiyonel teorisi (PBE-D3(BJ)) kullanılarak gerçekleştirilen bu çalışma, %5-8 oranındaki ılımlı katkılamanın adsorpsiyonu belirgin şekilde güçlendirdiğini ortaya koymaktadır. Özellikle bor katkısı elektrostatik çekim kuvveti üzerinden bağlanmayı artırırken, azot katkısı ağırlıklı olarak polarizasyon ve indüksiyon etkilerini yükseltmektedir. Bununla birlikte çalışmanın en çarpıcı bulgusu, yüksek dopant oranlarının grafen yüzey potansiyelinde bir 'elektronik pürüzsüzleşmeye' (electronic smoothing) yol açarak, bağlanma afinitesini beklenmedik bir şekilde zayıflatmasıdır. Elde edilen sonuçlar, güçlü ve kontrollü ilaç tutulumuna sahip grafen taşıyıcıların tasarlanmasında, %5-8 aralığındaki bir 'katkılama penceresinin' en uygun strateji olduğunu göstermektedir.

## Anahtar kelimeler

Sisplatin,
Grafen nanotaşıyıcılar,
Heteroatom katkılama,
İlaç Taşınımı,
Kovalent olmayan etkileşimler

## 1. INTRODUCTION

Graphene, composed of $sp^2$-hybridized carbon atoms arranged in a two-dimensional honeycomb lattice, has attracted considerable attention due to its exceptional physicochemical properties, including high mechanical strength, excellent electrical and thermal conductivity, chemical stability, and a large specific surface area [1–5]. In addition, many of graphene's inherent optical properties and the potential for electronically modifying those properties through the synthesis of quantum dots (GQDs) position graphene-derived materials as possible candidates for a wide range of biomedical applications [6–8]. Among them, drug delivery systems (DDS) are among the most notable because the nanometer size of graphene allows for more efficient loading of drugs onto graphene than into conventional vehicles, enhanced solubility of drugs, and improved pharmacokinetic profiles [9–11]. Moreover, the capacity to modify the surface functionality of graphene facilitates targeted drug delivery and limits systemic toxicity, providing unique benefits when compared to traditional drug delivery vehicles, especially in the delivery of drugs with narrow therapeutic windows [12–14]. However, pristine graphene's lack of polarity and low surface energy severely limit the ability of graphene to interact with biological fluids. Graphene doped with boron (B) or nitrogen (N) can be used to solve these problems, as doping creates polar functional groups on graphene, which can enhance the interaction of graphene with therapeutic agents via increased electrostatic attractions and hydrogen bonding attractions between molecules, as well as facilitate molecular dispersion stacking interactions [15]. The versatility in surface chemistry that results from doped graphene nanostructure makes them highly attractive to use in developing DDSs, which are both biologically compatible and capable of selectively delivering drugs to target cancer cells. [16,17]

.Nitrogen-doped graphene quantum dots (N-GQDs) are also capable of serving as multifunctional nanocarriers due to their high aqueous solubility, low toxicity, and ability to bind strongly to aromatic drugs [18,19]. Boron doping similarly enhances binding affinity by generating electron-deficient sites that serve as active adsorption centers [20,21]. Experimental evidence shows that doped graphene systems are indeed useful. Doping of graphene with boron was shown to increase the adsorption rate of amphetamine-like compounds. Additionally, N-GQDs were able to selectively kill cancer cells when loaded with methotrexate. The use of functionalized GQDs to deliver doxorubicin showed increased specificity and uptake in vitro [22,23]. Since its discovery by Rosenberg et al. [24], cisplatin has played a pivotal role in the treatment of several malignancies, including testicular, ovarian, lung, and bladder cancers [25–27]. However, the utility of cisplatin as a therapeutic agent is limited by the toxicity associated with it at higher doses and the development of drug-resistant tumors. Recent studies indicate that the delivery of cisplatin using nanocarriers (such as carbon-based systems) may help alleviate these problems [28,29]. Graphene-based carriers have shown improved intracellular uptake and therapeutic efficacy of cisplatin using either covalent attachment or non-covalent physisorption mechanisms to cisplatin. Specifically, the non-covalent adsorption of cisplatin onto π-rich graphene surfaces is energetically favored; therefore, doped graphene-based platforms may represent viable options for the delivery of cisplatin with lower systemic toxicity [30–32].

The aim of this study is to elucidate the noncovalent forces that govern cisplatin binding on doped carbon frameworks using a validated, dispersion-aware electronic-structure strategy. Within a single, internally consistent protocol that directly extends our prior collaborative research, PBE-D3(BJ) applied to both B- and N-doped graphene nano-prototypes provides reliable physisorption energetics and equilibrated geometries [30,32–34], while density-functional symmetry-adapted perturbation theory (DFT-SAPT) resolves the interaction into physically meaningful components. This combination maps how dopant identity reshapes the balance among dispersion, electrostatics, induction, and charge transfer in cisplatin–graphene complexes and relates these changes to concise geometric descriptors such as equilibrium contact distances and local contact motifs around the Pt center. The resulting mechanistic picture offers practical guidance for engineering doped-graphene carriers with stronger yet controlled binding to Pt-based drugs, highlighting dopant chemistry as a direct handle for tuning drug–surface interactions.

## 2. MATERIAL AND METHOD

Quantum chemical calculations were employed to systematically investigate the adsorption characteristics of cisplatin (CP) on a set of nitrogen– and boron–doped graphene nanofragments designed as potential drug delivery platforms. Initial geometry optimizations and interaction energy evaluations were performed within the framework of density functional theory (DFT), using the PBE exchange–correlation functional augmented with Grimme's D3 dispersion correction and Becke–Johnson damping [PBE-D3(BJ)] [35,36]. This level of theory has been validated for accurately modeling noncovalent interactions between CP and extended π-conjugated systems [30,32,33]. In these DFT calculations, the platinum center in the CP molecule was modeled using the Stuttgart–Dresden (SDD) [37] effective core potential, which incorporates scalar relativistic effects and efficiently treats core electrons. For all remaining atoms, the 6-311++G(2d,2p) [38] basis set was employed to ensure an accurate representation of valence electron distributions and polarization effects. All pristine and doped graphene prototypes (GPs) were first fully optimized at the PBE-D3(BJ) level without any geometrical constraints to obtain relaxed reference structures for each composition. Subsequently, CP–GP adsorption complexes were generated and optimized under the rigid monomer approximation [39]: during these complex optimizations, the GP framework was kept fixed at its pre-optimized geometry, while the cisplatin molecule was allowed to relax. The rigid monomer approximation was employed after noting that adsorption enthalpies on graphene are predominantly influenced by

interaction energies rather than structural deformations. This is in line with systems where London dispersion is the main force that draws things together.

To construct the doped graphene nanofragments, a pristine $C_{37}H_{16}$ cluster cut as a hydrogen-terminated graphene patch with mixed armchair/zigzag edges was used as the starting structure. Nitrogen and boron doping was systematically carried out by substituting one to six carbon atoms with N or B atoms, respectively, restricted to basal $sp^2$ carbon sites. This approach yielded twelve unique doped clusters: six nitrogen-doped structures ($C_{36}H_{15}N$, $C_{35}H_{16}N_2$, $C_{34}H_{15}N_3$, $C_{33}H_{16}N_4$, $C_{32}H_{15}N_5$, and $C_{31}H_{16}N_6$) and six boron-doped counterparts ($C_{36}H_{15}B$, $C_{35}H_{16}B_2$, $C_{34}H_{15}B_3$, $C_{33}H_{16}B_4$, $C_{32}H_{15}B_5$, and $C_{31}H_{16}B_6$). Optimization of all undoped and doped fragments was done to the PBE-D3(BJ) level in an unconstrained manner with no restrictions, thus establishing a consistent basis for comparison among compositions.

Energy decomposition analyses were conducted to provide a detailed understanding of the basic elements that determine CP – surface interaction using symmetry-adapted perturbation theory based on DFT (DFT-SAPT). [40,41]. These post-DFT computations were applied to five representative complexes: CP–$C_{37}H_{16}$, CP–$C_{35}H_{16}N_2$, CP–$C_{35}H_{16}B_2$, CP–$C_{31}H_{16}N_6$, and CP–$C_{31}H_{16}B_6$. CP–$C_{37}H_{16}$ represents the undoped reference system, CP–$C_{35}H_{16}N_2$ and CP–$C_{35}H_{16}B_2$ exhibit the strongest adsorption energies among the doped structures, while CP–$C_{31}H_{16}N_6$ and CP–$C_{31}H_{16}B_6$ correspond to the highest dopant concentrations (16%) within the cluster set. The atomic ratio of substituents (N or B) to the total lattice sites in the $C_{37}H_{16}$ model was used to figure these out. By changing the number of dopants from 1 to 6, a systematic concentration gradient (about 3% to 16%) was created to see how the electronics affected adsorption. In the case of DFT-SAPT, the PBE0 hybrid functional [42] was used to approximate the exchange–correlation energy contributions. Moreover, the δ(HF) (43) contribution has also been added to the DFT-SAPT energies as part of the induction term. The aug-cc-pVDZ-PP [44] basis set was employed for the platinum (Pt) atom, while the aug-cc-pVDZ (45) basis set was used for all other atoms in the system. To approximate the complete basis set (CBS) limit, the computed dispersion energy component was scaled by a factor of 1.1931, following the extrapolation protocol proposed in the literature [46]. Boys and Bernardi's counterpoise method [47] was employed to correct the Basis Set Superposition Error (BSSE) in interaction energies calculated using both DFT and DFT-SAPT methods. This made sure that noncovalent binding strengths were measured consistently and accurately.

The Gaussian 09 software suite [48] was used to do the geometry optimizations and all the DFT-level calculations. After that, the quantum chemistry program Molpro 2012 [49] was used to do the DFT-SAPT energy decomposition analyses. The software GaussView 5.0 [50] was used solely to visualize the results.

## 3. RESULTS

### 3.1 Structure and Energetics of Cisplatin Adsorption

For the initial modeling of the graphene-based nanocarrier, was selected the planar polycyclic aromatic hydrocarbon $C_{37}H_{16}$ due to its favorable balance between computational tractability and structural representativeness. This molecule is small enough for high-level quantum chemical calculations, which are necessary to accurately describe weak non-covalent interactions, such as stacking interactions and dispersion forces. It is also big enough to effectively mimic the extended π-conjugated surface of graphene and reduce edge effects from hydrogen atoms on the outside. Its flat shape makes interactions that are physically meaningful and stable possible, especially when the adsorbed molecule is lined up parallel to the graphene surface. This is a configuration that is known to increase van der Waals contributions. $C_{37}H_{16}$ was successfully used in our previous work [33] as a model graphene to study how gold(I) monocarbene complexes stick to it. In modeling the adsorption behavior of cisplatin on the graphene prototype, it was considered that several spatial arrangements between the drug and the nanocarrier surface are possible, including both parallel and perpendicular configurations. A preliminary conformational search was performed by initializing the cisplatin molecule in various horizontal orientations relative to the dopant sites to identify the energy minima. A systematic exploration of perpendicular or tilted configurations was not prioritized, as maximizing the ligand-surface contact area is expected to be critical for dispersion-driven adsorption. Furthermore, previous high-level computational investigations consistently demonstrate that parallel configurations of cisplatin on graphene-like surfaces lead to the most favorable noncovalent interactions [32,51].

To evaluate how heteroatom doping modulates the interaction between cisplatin (CP) and graphene-based carriers, adsorption energies and equilibrium distances were computed for a series of nitrogen- and boron-doped graphene fragments, alongside the undoped $C_{37}H_{16}$ reference. As summarized in Table 1, doping significantly enhances the binding affinity of cisplatin in most cases, with boron-doped systems generally exhibiting stronger interactions than their nitrogen-doped counterparts at comparable doping levels. The undoped graphene model ($C_{37}H_{16}$), which exhibits an interaction energy of –701.2 meV and an equilibrium distance of 3.50 Å, serves as a valid and computationally efficient prototype. This cluster lies in size between ovalene ($C_{32}H_{14}$) and circumcoronene ($C_{54}H_{18}$), two representative polycyclic aromatic hydrocarbons (PAHs) employed in the benchmark study by Cuevas-Flores et al. [32]. As a result, the computed interaction energy for CP–$C_{37}H_{16}$ falls reasonably between those obtained for these two systems, reinforcing the physical relevance of the chosen model. Specifically, the CP–ovalene complex was reported to exhibit a BSSE-corrected interaction energy of –664.9 meV (–778.9 meV uncorrected) with an equilibrium distance around 3.5 Å,

which is in excellent agreement with the results obtained herein results for CP–$C_{37}H_{16}$.

**Table 1:** Equilibrium interaction distances, doping percentages, and BSSE-corrected interaction energies calculated at the PBE-D3(BJ)/6-311++G(2d,2p) + SDD level of theory for undoped and N/B-doped graphene systems.

| Structures | % Doping | d (Å) | Energy (meV) |
|---|---|---|---|
| CP – $C_{37}H_{16}$ | 0 | 3.5 | -701.20 |
| CP – $C_{36}H_{15}N$ | 3 | 3.37 | -899.81 |
| CP – $C_{35}H_{16}N_2$ | 5 | 3.50 | -1085.84 |
| CP – $C_{34}H_{15}N_3$ | 8 | 3.33 | -961.82 |
| CP – $C_{33}H_{16}N_4$ | 11 | 3.36 | -898.50 |
| CP – $C_{32}H_{15}N_5$ | 13 | 3.38 | -859.48 |
| CP – $C_{31}H_{16}N_6$ | 16 | 3.56 | -934.50 |
| CP – $C_{36}H_{15}B$ | 3 | 3.35 | -992.17 |
| CP – $C_{35}H_{16}B_2$ | 5 | 3.51 | -1221.57 |
| CP – $C_{34}H_{15}B_3$ | 8 | 3.21 | -1113.16 |
| CP – $C_{33}H_{16}B_4$ | 11 | 3.27 | -1074.13 |
| CP – $C_{32}H_{15}B_5$ | 13 | 3.22 | -921.05 |
| CP – $C_{31}H_{16}B_6$ | 16 | 3.25 | -986.96 |

When comparing the current results to other DFT-based approaches, such as the study by Munny et al. [51], distinct methodological differences emerge. In their work, the authors employed the GGA/PBE functional combined with Tkatchenko–Scheffler (TS) dispersion corrections and a double numerical plus polarization (DNP) basis set within the DMol³ framework. While BSSE corrections were applied in their study, the variations in results may be attributed to the specific choice of computational parameters; the present work utilizes the PBE-D3(BJ) functional and the 6-311++G(2d,2p) + SDD basis set. These methodological distinctions are reflected in the reported adsorption energy for cisplatin onto pristine graphene of –0.85 eV (–850 meV), illustrating the sensitivity of such energetic values to the treatment of dispersion and basis set selection. The reported adsorption energy exceeds the BSSE-corrected interaction energy found by Cuevas-Flores et al. (–749.0 meV) for CP–$C_{150}H_{30}$. This system is nearly four times larger in surface area than the graphene prototype used by them. Therefore, it appears that their large reported adsorption energy may be indicative of an overestimation caused by the lower-level functional and limited basis set. Also, this shows how important it is to select good-quality theoretical models and basis sets when simulating physical adsorption processes that depend on a balance between dispersion forces and electrostatics.

The optimized adsorption geometries of the nitrogen-doped graphene complexes investigated in this study are depicted in Figure 1, illustrating the relative spatial arrangement of cisplatin with respect to the dopant sites. For nitrogen doping, the minimum adsorption distance varies modestly between 3.33 and 3.56 Å depending on the doping level. At relatively low to moderately high dopant concentrations (3-8%), a slight reduction in the distance is observed, which decreases to 3.33 Å at 8% N-doping. The trend indicates that localized enhancement of either electrostatic or polarization interactions due to moderate nitrogen incorporation can allow the cisplatin molecule to be closer to the graphene surface. At the maximum doping concentration (16%), a greater separation of 3.56 Å appears, suggesting some form of structural distortions or a decrease in the available surface–ligand contact area as a result of electronic repulsion or too much disruption to the conjugation of the carbon framework.

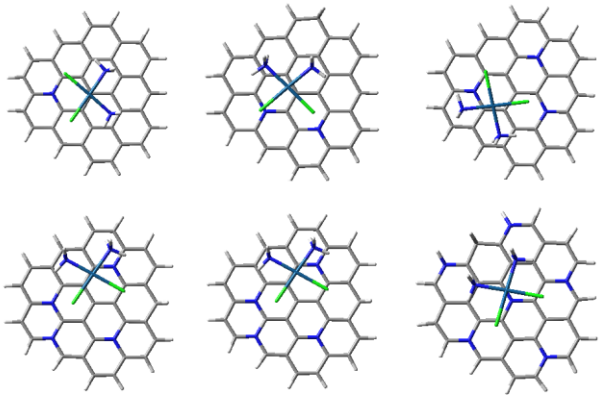

**Figure 1.** Top views of the nitrogen-doped graphene complexes optimized using DFT calculations at the PBE-D3(BJ)/6-311++G(2d,2p) + SDD level of theory. The structures are presented in order of increasing nitrogen doping concentration.

Figure 2 shows the optimized geometries of the boron-doped graphene complexes, highlighting the characteristic positioning of cisplatin relative to the electron-deficient boron sites. In contrast, boron-doped systems display a more pronounced and consistent reduction in adsorption distance across doping levels. Even at 3% B-doping, the distance decreases to 3.35 Å, reaching a minimum of 3.21 Å at 8% doping.

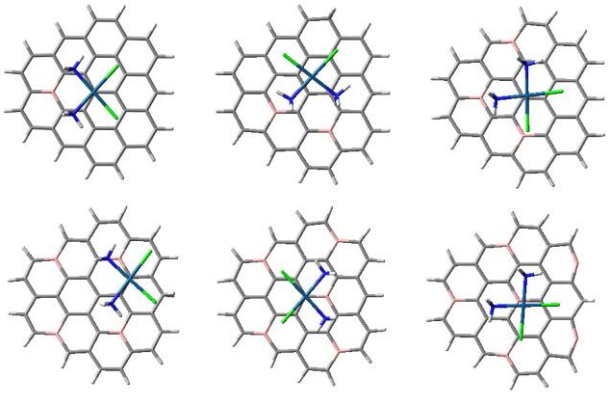

**Figure 2.** Top views of the boron-doped graphene complexes optimized using DFT calculations at the PBE-D3(BJ)/6-311++G(2d,2p) + SDD level of theory. The structures are presented in order of increasing boron doping concentration.

Notably, the distance remains below 3.30 Å at all higher B-doping levels (except at 5%, where it briefly increases to 3.51 Å), indicating a consistent trend in structural proximity despite minor deviations.

To further evaluate the preservation of the intrinsic geometry of cisplatin upon adsorption, critical bond lengths and angles were compared between the gas-phase monomer and surface-bound complexes. At the PBE-D3(BJ)/6-311++G(2d,2p) + SDD level of theory, geometry optimizations reproduce the experimental structural parameters of cisplatin with great accuracy. Table 2 shows the bond distances and angular deviations that are important for both the isolated and adsorbed species. This makes it easy to compare the structural integrity of the two species in different environments. In particular, the computed Pt–N and Pt–Cl bond lengths in the gas-phase monomer deviate by only ~0.06 Å and ~0.01 Å, respectively, from crystallographic values (52), while key angular descriptors such as N–Pt–Cl and Cl–Pt–Cl differ by less than 3°, underscoring the reliability of the chosen computational method. Notably, the internal geometry of cisplatin remains essentially unaltered upon physisorption onto both pristine ($C_{37}H_{16}$) and doped ($C_{35}H_{16}N_2$, $C_{35}H_{16}B_2$) graphene models. The Pt–N, Pt–Cl, and N–H bond distances exhibit negligible variations across all adsorbed complexes compared to the isolated monomer, suggesting that the adsorption process does not significantly distort the coordination environment of the platinum center.

**Table 2:** Selected bond lengths (Å) and bond angles (°) of cisplatin in the experimental crystal structure, as an isolated monomer, and in complexes with pristine ($C_{37}H_{16}$) and doped graphene models ($C_{35}H_{16}N_2$ and $C_{35}H_{16}B_2$), optimized at the PBE-D3(BJ)/6-311++G(2d,2p) + SDD level of theory. Experimental X-ray data [52] are included for comparison

| Geometric parameters | Monomer | | Complex | | |
|---|---|---|---|---|---|
| | Crystal Structure [52] | Calculated | CP−$C_{37}H_{16}$ | CP−$C_{35}H_{16}N_2$ | CP−$C_{35}H_{16}B_2$ |
| Pt-N | 2.03 | 2.09 | 2.09 | 2.09 | 2.09 |
| Pt-Cl | 2.31 | 2.32 | 2.32 | 2.39 | 2.39 |
| N-H | 0.91 | 1.03 | 1.03 | 1.04 | 1.03 |
| N-Pt-N | 91.8 | 99.4 | 97.8 | 95.6 | 96.4 |
| N-Pt-Cl1 | 178.9 | 178.3 | 178.8 | 178.8 | 179.1 |
| N-Pt-Cl2 | 87.6 | 82.3 | 83.1 | 84.9 | 84.4 |
| Cl-Pt-Cl | 92.6 | 95.9 | 95.8 | 94.6 | 94.8 |
| Pt-N-H | 109.5 | 114.2 | 113.8 | 110.4 | 111.2 |

The only appreciable structural difference among the complexes appears in the N–Pt–N bond angle, which shows a slight contraction (from 99.4° to as low as 95.6°) depending on the nature of the underlying graphene substrate. This subtle variation may be attributed to the electrostatic sensitivity of the cisplatin nitrogen atoms, which carry a partial positive charge and are therefore more responsive to local electronic perturbations induced by heteroatom doping in the graphene sheet. In particular, nitrogen or boron dopants can locally polarize the π-system of graphene, leading to asymmetric noncovalent interactions that slightly modulate the bite angle at the platinum center. Importantly, these geometric perturbations remain minor and do not compromise the structural integrity of the drug molecule upon surface adsorption.

Interestingly, the structures exhibiting the strongest interaction energies in each doping class—namely the undoped system ($C_{37}H_{16}$), the 2N-doped system ($C_{35}H_{16}N_2$), and the 2B-doped system ($C_{35}H_{16}B_2$)—all share a common feature: the equilibrium adsorption distance is approximately 3.50 Å in all three cases. This convergence suggests that the optimal spatial alignment between cisplatin and the graphene surface is largely governed by molecular shape and a parallel, dispersion-favorable contact geometry, rather than purely electronic effects. Remarkably, this same equilibrium distance (3.50 Å) was also observed in our previous work [33] involving the physisorption of gold(I) monocarbene complexes on the $C_{37}H_{16}$ prototype. There too, high-level DFT-SAPT and MP2C calculations confirmed that 3.5 Å represented the optimal van der Waals contact distance for parallel orientations.

### 3.2 Energy Decomposition and Electronic Charge Topography

To establish both the reliability and the physical makeup of the cisplatin–graphene interaction, density functional symmetry adapted perturbation theory (DFT-SAPT) calculations were carried out for five representative adsorption complexes. The set comprises the undoped $C_{37}H_{16}$ fragment and four doped structures, namely $C_{35}H_{16}N_2$ and $C_{35}H_{16}B_2$ as the strongest binders within the N and B series, and $C_{31}H_{16}N_6$ and $C_{31}H_{16}B_6$ as the highest dopant loadings considered. DFT-SAPT serves two goals in this study. First, it provides an independent interaction-energy framework that was used to cross validate the adsorption energies obtained with PBE-D3(BJ) and to verify that the observed stability trends are not tied to a single electronic-structure model. Second, it supplies a component resolved description of the interaction as a function of dopant identity and concentration, separating electrostatics, exchange repulsion, induction (polarization), and dispersion. All SAPT calculations were performed on the PBE-D3(BJ) optimized geometries with a consistent monomer partition between cisplatin and

the graphene fragment, which enables direct comparison of SAPT totals and decompositions across the selected complexes. The resulting totals and component partitions are collected in Table 3 and form the methodological basis for the analysis developed in the subsequent sections.

**Table 3:** DFT-SAPT/CBS energy decomposition of the interaction between cisplatin and undoped or N/B-doped $C_{37}H_{16}$ graphene models (in meV).

| | **CP–$C_{37}H_{16}$** | **CP–$C_{35}H_{16}N_2$** | **CP–$C_{31}H_{16}N_6$** | **CP–$C_{35}H_{16}B_2$** | **CP–$C_{31}H_{16}B_6$** |
|---|---|---|---|---|---|
| Electrostatic | -362.4 | -652.1 | -605.2 | -934.1 | -789.8 |
| Exchange repulsion | 903.7 | 1325.8 | 1322.4 | 1311.3 | 1587.3 |
| Induction | -259.2 | -781.4 | -485.7 | -547.2 | -476.2 |
| Dispersion [a] | -1069.8 | -1258.6 | -1210.3 | -1234.1 | -1349.5 |
| Total | -787.7 | -1366.3 | -978.8 | -1404.1 | -1028.2 |

[a] $E_d$ value was multiplied by 1.1931 for the extrapolation to the CBS limit [46]

For the CP–$C_{37}H_{16}$ complex, which represents the undoped graphene prototype, the total interaction energy was calculated to be –787.7 meV. Among the contributing terms, dispersion dominates the attractive interactions (–1069.8 meV), consistent with the large π-electron cloud of the extended sp²-carbon framework. Electrostatic (–362.4 meV) and induction (–259.2 meV) contributions are both present but significantly smaller, while the exchange repulsion (+903.7 meV) partially offsets the attractive terms. This dispersion-dominated, weakly electrostatic profile is typical of van der Waals physisorption on neutral, nonpolar π-conjugated surfaces.

In contrast to the pristine graphene model, heteroatom doping significantly alters the energetic balance of noncovalent interactions. For the nitrogen-doped complex (CP–$C_{35}H_{16}N_2$), the total SAPT interaction energy increases substantially to –1366.3 meV. This enhancement is primarily driven by a marked increase in the induction component (–781.4 meV), along with a strengthened dispersion contribution (–1258.6 meV). Interestingly, despite nitrogen's higher electronegativity and the presence of an extra valence electron compared to carbon, the electrostatic component exhibits only a moderate increase (–652.1 meV). Examining the molecular electrostatic potential (MEP) maps makes this initially surprising result more understandable. Despite adding an additional electron to the system, nitrogen atoms withdraw π-electron density from the surrounding conjugated graphene ring due to their higher electronegativity. The MEP surfaces of cisplatin, undoped $C_{37}H_{16}$, and nitrogen-doped systems are shown in Figure 3. The redistribution of electrons leads to an increase in partial positive charge in the vicinity of carbon atoms that are close to the dopants, as well as the opposite effect for more remote regions, which become electron-rich through the process of delocalization. The redistribution of charge creates a non-uniform electrostatic environment (as observed by MEP), where areas closest to the dopant are positively charged, and areas further from the dopant become negatively charged.

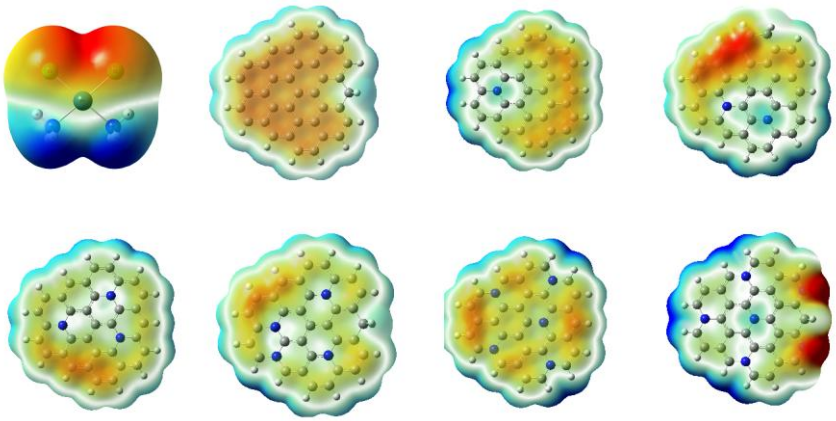

**Figure 3**: MEP maps on the 0.0004 $e^{-}\cdot Bohr^{-3}$ isodensity surface for isolated cisplatin, pristine $C_{37}H_{16}$, and N-doped graphene substrates ordered by increasing N content. (Color scale: −0.03 to +0.03 a.u; red = electron-rich, blue = electron-deficient)

In the optimized geometry of the CP–$C_{35}H_{16}N_2$ complex, this asymmetric charge distribution governs the orientation of cisplatin. The electron-rich $Cl^-$ ligands align with the electropositive carbon atoms adjacent to nitrogen, while the $NH_3$ groups, which are relatively electron-poor, orient toward the distant, electron-rich areas of the graphene surface. This arrangement favors polarization effects over static electrostatic attraction. As a result, the induction term is the most important part of the increased interaction energy. Induction is the stabilization that occurs when two molecules interact with each other, and their electron clouds respond to each other's electric fields. In this case, the polarizable π-system of nitrogen-doped graphene changes in response to the fields created by the dipolar $NH_3$ and $Cl^-$ groups in cisplatin. This causes strong second-order polarization effects, which means that induction, not just charge complementarity, is what makes the binding stronger.

The total SAPT interaction energy for the boron-doped system (CP–$C_{35}H_{16}B_2$) was –1404.1 meV, which was the best binding of all the complexes we looked at. The electrostatic part of the CP–$C_{35}H_{16}B_2$ complex is much stronger than the nitrogen-doped part, adding –934.1 meV to the total interaction energy. This is accompanied by significant dispersion (–1234.1 meV) and moderate induction (–547.2 meV) terms, indicating a balanced interaction of noncovalent forces. As a result of boron having fewer valence electrons than carbon and being less electronegative, when boron is substituted into the graphene structure, it creates local areas of electron deficiency inside the π-conjugated system. The π-electron density is redistributed to satisfy the electron deficiency created by boron; thus, π-electrons are attracted to the region of the graphene lattice where the boron is located, resulting in localized areas of higher electron density at the boron sites. Conversely, the carbon atoms located further away from the boron atom will have lost some electron density and become relatively electropositive. These changes can be visualized with MEP (molecular electrostatic potential) maps that show the potential to be significantly negative near each boron atom and positive in the outer periphery of the graphene fragment, as seen in Figure 4.

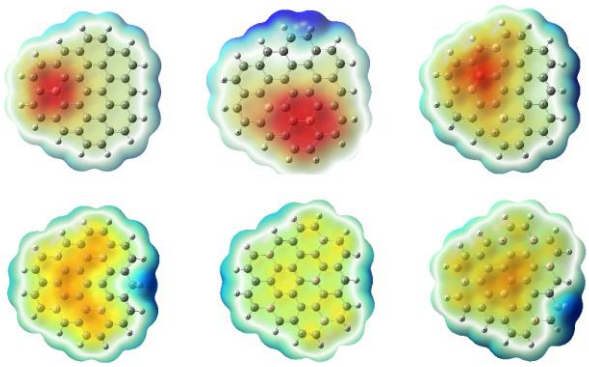

**Figure 4**: MEP maps on the 0.0004 $e^{-}$·$Bohr^{-3}$ isodensity surface for isolated cisplatin and B-doped $C_{37}H_{16}$ substrates at increasing B content, showing how p-type doping redistributes the surface potential. Color scale: −0.03 to +0.03 a.u.; red = electron-rich, blue = electron-deficient

Consequently, this polarization drives the orientation of cisplatin within the CP–$C_{35}H_{16}B_2$ complex. As the $NH_3$ ligands have a partial positive character compared to the rest of the cisplatin molecule, they are positioned for optimal electrostatic attraction towards electron-rich zones surrounding the boron dopants on the $C_{35}H_{16}B_2$. In contrast, the electron-rich chloride ligands are placed for electrostatic attraction toward the electron-deficient zones on the graphene surface, which are located at a greater distance from the boron atoms. The spatial compatibility of the polarized graphene surface with respect to the dipole moments of cisplatin facilitates an enhanced bonding interaction. The energy decomposition profile confirms this behavior: among all systems studied, the CP–$C_{35}H_{16}B_2$ complex has the highest electrostatic contribution of all the systems studied, which is clearly higher than that of both the undoped and N-doped analogues. The electron density around the boron sites was also smooth and localized, which made the exchange repulsion (1311.3 meV) a little less strong and helped to stabilize the complex even more. These findings underscore the essential function of p-type doping in modifying the electronic environment of graphene to enhance drug–carrier interactions through improved electrostatic complementarity.

Moderate levels of heteroatom doping enhance the interaction between cisplatin and graphene derivatives; however, elevated concentrations of dopants (six substituents or 16% doping) markedly diminish the total binding energy. This effect happens whether the system has boron or nitrogen as dopants. You can look at the distribution of electrostatic potential, SAPT energy components, and the equilibrium geometry to see what happens. In the highly boron-doped system (CP–$C_{31}H_{16}B_6$), the total SAPT interaction energy decreases to –1021.4 meV. Although this structure corresponds to the highest boron doping level (six B atoms, 16%), it does not exhibit the weakest binding affinity. As shown in Table 1, the lowest adsorption energy among the boron-doped complexes is observed for CP–$C_{32}H_{15}B_5$ (–921.1 meV), which contains five boron atoms, corresponding to approximately 13% doping. Thus, the introduction of an excess of B-dopant atoms reduces the local electrostatic difference at the graphene surface due to the delocalization of π-electrons over the entire graphene surface. The individual effects of all boron atoms, inducing a localized polarization effect in their vicinity by removing electrons from their adjacent carbon atoms, are collectively merged and thus neutralized as a result of the presence of five or more dopants. These collective effects reduce the total electrostatic energy (–789.8 meV) and make the molecular electrostatic potential (MEP) surface more uniform. The reduction of electrostatic interaction between the complexes is apparent when examining the MEP image of the CP–$C_{32}H_{15}B_5$ complex; the latter does not exhibit the typical electropositive and electronegative areas required for high non-covalent interaction strength. Although the dispersion contribution is very large (–1349.5 meV), it cannot counteract the decreased electrostatic contributions and therefore results in a global decrease in the interaction strengths.

A similar trend is observed in nitrogen-doped systems. The CP–$C_{31}H_{16}N_6$ complex, which features six nitrogen atoms (16% doping), yields a total SAPT interaction energy of –978.7 meV. However, the weakest DFT-calculated adsorption energy is obtained for the CP–$C_{32}H_{15}N_5$ complex (–859.5 meV), which incorporates five nitrogen dopants (13% doping). This result shows that adding a lot of nitrogen makes the graphene surface less polarizable. At low concentrations, nitrogen, which is more electronegative and has an extra valence electron compared to carbon, increases charge asymmetry and induction interactions. However, as the number of dopants increases, the surface becomes uniformly electron-deficient. This reduces local polarization effects and lowers induction energy contributions from –781.4 meV in the 2N system to –485.7 meV in the 6N system. The MEP surface of CP–$C_{32}H_{15}N_5$ clearly shows how electrostatic variation has flattened and polarizable regions have disappeared. The charge inhomogeneity that is typical of this surface is much less noticeable.

When combined with the results from the SAPT and MEP analyses, the findings herein demonstrate that although the use of heteroatoms is an efficient method to increase interaction between drugs and the surface, there is a specific concentration at which heteroatom doping becomes ineffective. In particular, the high doping levels of either boron or nitrogen into the graphene structure reduce the heterogeneity of the surface's electronic environment, resulting in decreased electrostatic and inductive forces and therefore reduced surface adsorption. Thus, the optimal amount of doping required to maximize non-covalent binding of the adsorbate to the substrate must be determined based on maximizing the charge difference between the substrate and the adsorbate, and therefore the greatest degree of non-covalent binding

## 4. DISCUSSION AND CONCLUSION

The physisorption mechanism of cisplatin on pristine and heteroatom-doped graphene nano fragments was studied through the use of dispersion corrected (PBE-D3(BJ)) calculations as well as through a DFT-SAPT component resolved analysis of structural and energetic results. The results demonstrate that doping with heteroatoms can be used to modulate the interaction between drugs and surface material, and the magnitude of the modulation is dependent upon the type of dopant and the level of doping. More specifically, it was demonstrated that the boron-doped surfaces have a higher level of interaction with cisplatin than the nitrogen-doped surfaces because of increased electrostatic complementarity in addition to an increase in induction effects from nitrogen doping. Although dispersion is still the primary driving force for adsorption onto the surface, the localized electronic perturbation caused by the dopant increases the total binding energy.

A crucial insight from the analysis is the existence of a saturation point for the doping benefit. Moderate doping levels (approx. 3–8%) strengthen adsorption by inducing surface charge heterogeneity, whereas higher loadings (13–16%) result in an "electronic smoothing" of the surface potential. This smoothing happens when the electrostatic potential across the lattice becomes more uniform because overlapping electronic clouds from nearby dopant sites reduce the localized gradients that make strong interaction energies possible. As a result, this effect makes the London dispersive forces that keep things stable weaker. Consequently, an optimal design window of approximately 5–8% heteroatom content is proposed to maximize noncovalent binding. Since the data presented herein are limited to gas-phase interactions to isolate intrinsic electronic effects, future studies should focus on comprehensive thermodynamic profiling, including solvation and entropy effects, to accurately predict bioavailability and drug release dynamics in biological environments.

## REFERENCES


[1] Castro Neto, A.H.; Guinea, F.; Peres, N.M.R.; Novoselov, K.S.; Geim, A.K. The Electronic Properties of Graphene. *Rev Mod Phys* 2009, *81*, 109–162, doi:10.1103/RevModPhys.81.109.

[2] Li, S.; Luo, Z.; Tu, H.; Zhang, H.; Deng, W.; Zou, G.; Hou, H.; Ji, X. Corrigendum to 〈N,S-Codoped Carbon Dots as Deposition Regulating Electrolyte Additive for Stable Lithium Metal Anode〉 [Energy Storage Materials 42 (2021) 679–686]. *Energy Storage Mater* 2021, *43*, 595–596, doi:10.1016/j.ensm.2021.10.015.

[3] Guo, R.; Miao, Q.; Xu, Y. Review of Graphene Applications in Electric Vehicle Thermal Management Systems. *World Electric Vehicle Journal* 2025, *16*, 166, doi:10.3390/wevj16030166.

[4] Han, Z.; Ruan, X. Thermal Conductivity of Monolayer Graphene: Convergent and Lower than Diamond. *Phys Rev B* 2023, *108*, L121412, doi:10.1103/PhysRevB.108.L121412.

[5] Ramezani, M.J.; Rahmani, O. A Review of Recent Progress in the Graphene Syntheses and Its Applications. *Mechanics of Advanced Materials and Structures* 2024, 1–33, doi:10.1080/15376494.2024.2420911.

[6] Jan, A.; Batool, M.; Akram, S.; Malik, A.H.; Khanday, W.A.; Wani, W.A.; Sheikh, R.A.; Rather, J.A.; Kannan, P. Functionalized Graphene Quantum Dots (FGQDs): A Review of Their Synthesis, Properties, and Emerging Biomedical Applications. *Carbon Trends* 2025, *18*, 100442, doi:10.1016/j.cartre.2024.100442.

[7] Rasheed, P.A.; Ankitha, M.; Pillai, V.K.; Alwarappan, S. Graphene Quantum Dots for Biosensing and Bioimaging. *RSC Adv* 2024, *14*, 16001–16023, doi:10.1039/D4RA01431F.

[8] Barati, F.; Avatefi, M.; Moghadam, N.B.; Asghari, S.; Ekrami, E.; Mahmoudifard, M. A Review of Graphene Quantum Dots and Their Potential Biomedical Applications. *J Biomater Appl* 2023, *37*, 1137–1158, doi:10.1177/08853282221125311.

[9] Kaur, A.; Babaliari, E.; Bolanos-Garcia, V.M.; Kefalogianni, M.; Psilodimitrakopoulos, S.; Kavatzikidou, P.; Ranella, A.; Ghorbani, M.; Stratakis, E.; Eskin, D.G.; et al. Assessment of Aqueous Graphene as a Cancer Therapeutics Delivery System. *Sci Rep* 2025, *15*, 15396, doi:10.1038/s41598-025-98406-0.

[10] Sadeghi, M. Graphene Oxide Nanocarriers for Effective Drug Delivery in Breast Cancer Treatment. *International Journal of Materials Science and Applications* 2024, *13*, 41–47, doi:10.11648/j.ijmsa.20241303.12.

[11] Osorio, H.M.; Castillo-Solís, F.; Barragán, S.Y.; Rodríguez-Pólit, C.; Gonzalez-Pastor, R. Graphene Quantum Dots from Natural Carbon Sources for Drug and Gene Delivery in Cancer Treatment. *Int J Mol Sci* 2024, *25*, 10539, doi:10.3390/ijms251910539.

[12] Dash, B.S.; Lu, Y.-J.; Huang, Y.-S.; Chen, J.-P. Chitosan-Coated Magnetic Graphene Oxide for Targeted Delivery of Doxorubicin as a Nanomedicine Approach to Treat Glioblastoma. *Int J Biol Macromol* 2024, *260*, 129401, doi:10.1016/j.ijbiomac.2024.129401.

[13] Liao, R.; Zhang, Y.; Mao, W. Functionalized Graphene Oxide NPs as a Nanocarrier for Drug Delivery System in Quercetin/ Lurbinectedin as Dual Sensitive Therapeutics for A549 Lung Cancer Treatment. *Heliyon* 2024, *10*, e31212, doi:10.1016/j.heliyon.2024.e31212.

[14] Lima-Sousa, R.; Melo, B.L.; Mendonça, A.G.; Correia, I.J.; de Melo-Diogo, D. Hyaluronic Acid-Functionalized Graphene-Based Nanohybrids for Targeted Breast Cancer Chemo-Photothermal Therapy. *Int J Pharm* 2024, *651*, 123763, doi:10.1016/j.ijpharm.2023.123763.

[15] Opi, M.H.; Ahmed, T.; Swarna, M.R.; Piya, A.A.; Shamim, S.U.D. Assessment of the Drug Delivery Potential of Graphene, Boron Nitride and Their in-Plane Doped Structures for Hydroxyurea Anti-Cancer Drug *via* DFT Study. *Nanoscale Adv* 2024, *6*, 5042–5054, doi:10.1039/D4NA00428K.

[16] Zhu, H.; Zhou, B.; Chan, L.; Du, Y.; Chen, T. Transferrin-Functionalized Nanographene Oxide for Delivery of Platinum Complexes to Enhance Cancer-Cell Selectivity and Apoptosis-Inducing Efficacy. *Int J Nanomedicine* 2017, *Volume 12*, 5023–5038, doi:10.2147/IJN.S139207.

[17] Feng, S.; Pan, J.; Li, C.; Zheng, Y. Folic Acid-Conjugated Nitrogen-Doped Graphene Quantum Dots as a Fluorescent Diagnostic Material for MCF-7 Cells. *Nanotechnology* 2020, *31*, 135701, doi:10.1088/1361-6528/ab5f7f.

[18] Khodadadei, F.; Safarian, S.; Ghanbari, N. Methotrexate-Loaded Nitrogen-Doped Graphene Quantum Dots Nanocarriers as an Efficient Anticancer Drug Delivery System. *Materials Science and Engineering: C* 2017, *79*, 280–285, doi:10.1016/j.msec.2017.05.049.

[19] Frieler, M.; Pho, C.; Lee, B.H.; Dobrovolny, H.; Akkaraju, G.R.; Naumov, A. V. Effects of Doxorubicin Delivery by Nitrogen-Doped Graphene Quantum Dots on Cancer Cell Growth: Experimental Study and Mathematical Modeling. *Nanomaterials* 2021, *11*, 140, doi:10.3390/nano11010140.

[20] Güven, G.K.; Okur, M.E.; Ayla, Ş.; Çalışkan, G.; Al, M.N.; Gülüm, L.; Tutar, Y.; Okur, N.Ü.; Değim, İ.T. Boron-Doped Carbon Quantum Dots: A Biocompatible Nanoplatform for Targeted Cancer Theranostics. *Int J Pharm* 2025, *679*, 125745, doi:10.1016/j.ijpharm.2025.125745.

[21] Li, W.; Zhang, L.; Jiang, N.; Chen, Y.; Gao, J.; Zhang, J.; Yang, B.; Liu, J. Fabrication of Orange Fluorescent Boron-Doped Graphene Quantum Dots for Al3+ Ion Detection. *Molecules* 2022, *27*, 6771, doi:10.3390/molecules27196771.

[22] Yanikoglu, R.; Karakas, C.Y.; Ciftci, F.; Insel, M.A.; Karavelioglu, Z.; Varol, R.; Yilmaz, A.; Cakir, R.; Uvet, H.; Ustundag, C.B. Development of Graphene Oxide-Based Anticancer Drug Combination Functionalized with Folic Acid as Nanocarrier for Targeted Delivery of Methotrexate. *Pharmaceutics* 2024, *16*, 837, doi:10.3390/pharmaceutics16060837.

[23] Zhao, C.; Song, X.; Liu, Y.; Fu, Y.; Ye, L.; Wang, N.; Wang, F.; Li, L.; Mohammadniaei, M.; Zhang, M.; et al. Synthesis of Graphene Quantum Dots and Their Applications in Drug Delivery. *J Nanobiotechnology* 2020, *18*, 142, doi:10.1186/s12951-020-00698-z.

[24] Rosenberg, B. Cisplatin: Its History and Possible Mechanisms of Action. In *Cisplatin*; Elsevier, 1980; pp. 9–20.

[25] Stelwagen, J.; Lubberts, S.; Steggink, L.C.; Steursma, G.; Kruyt, L.M.; Donkerbroek, J.W.; van Roon, A.M.; van Gessel, A.I.; van de Zande, S.C.; Meijer, C.; et al. Vascular Aging in Long-Term Survivors of Testicular Cancer More than 20 Years after Treatment with Cisplatin-Based Chemotherapy. *Br J Cancer* 2020, *123*, 1599–1607, doi:10.1038/s41416-020-01049-3.

[26] Zoń, A.; Bednarek, I. Cisplatin in Ovarian Cancer Treatment—Known Limitations in Therapy Force New Solutions. *Int J Mol Sci* 2023, *24*, 7585, doi:10.3390/ijms24087585.

[27] Ranasinghe, R.; Mathai, M.L.; Zulli, A. Cisplatin for Cancer Therapy and Overcoming Chemoresistance. *Heliyon* 2022, *8*, e10608, doi:10.1016/j.heliyon.2022.e10608.

[28] Rahnamaei Rahchamandi, S.Y.; Kazemi-Beydokhti, A.; Mirhadi, E.; Gheybi, F.; Askarizadeh, A.; menna, E.; Jaafari, M.R.; Alavizadeh, S.H. Engineered Hybrid Carbon Nanohorns-Lipid Platforms for the Delivery of Cisplatin to the Colorectal Cancer. *J Drug Deliv Sci Technol* 2024, *100*, 106101, doi:10.1016/j.jddst.2024.106101.

[29] Beheshtizadeh, N.; Kolahi Azar, H.; Seraji, A.A.; Zarei, M.; Hajian Monfared, M.; Mahheidari, N.; Darghiasi, S.F.; Afandideh, F.; Badihi, E.; Tabatabaei, S.Z. Cancer-Affected Tissue Regeneration Employing Cisplatin-Loaded Polymeric Nanoplatforms. *Biomedicine & Pharmacotherapy* 2025, *189*, 118250, doi:10.1016/j.biopha.2025.118250.

[30] Cuevas-Flores, M. del R.; Bartolomei, M.; García-Revilla, M.A.; Coletti, C. Interaction and Reactivity of Cisplatin Physisorbed on Graphene Oxide Nano-Prototypes. *Nanomaterials* 2020, *10*, 1074, doi:10.3390/nano10061074.

[31] Pineda-Urbina, K.; Kudur Jayaprakash, G.; Flores-Moreno, R.; Hernandez-Fuentes, G.A.; Gómez-Sandoval, Z.; Flores-Álvarez, J.M.; González-Ramírez, H.N.; Cervantes-Trujillo, C.H.; Manohara Sakamma, K. DFT-Guided Insights into Cisplatin Adsorption on Graphene and Asparagine-Modified Graphene. *The Journal of Physical Chemistry C* 2025, doi:10.1021/acs.jpcc.5c00624.

[32] Cuevas-Flores, M. del R.; Garcia-Revilla, M.A.; Bartolomei, M. Noncovalent Interactions between Cisplatin and Graphene Prototypes. *J Comput Chem* 2018, *39*, 71–80, doi:10.1002/jcc.24920.

[33] Orek, C.; Bartolomei, M.; Coletti, C.; Bulut, N. Graphene as Nanocarrier for Gold(I)-Monocarbene Complexes: Strength and Nature of Physisorption. *Molecules* 2023, *28*, 3941, doi:10.3390/molecules28093941.

[34] Araujo, R.B.; Rodrigues, G.L.S.; dos Santos, E.C.; Pettersson, L.G.M. Adsorption Energies on Transition Metal Surfaces: Towards an Accurate and

Balanced Description. *Nat Commun* 2022, *13*, 6853, doi:10.1038/s41467-022-34507-y.

[35] Grimme, S.; Ehrlich, S.; Goerigk, L. Effect of the Damping Function in Dispersion Corrected Density Functional Theory. *J Comput Chem* 2011, *32*, 1456–1465, doi:10.1002/jcc.21759.

[36] Perdew, J.P.; Burke, K.; Ernzerhof, M. Generalized Gradient Approximation Made Simple. *Phys Rev Lett* 1996, *77*, 3865–3868, doi:10.1103/PhysRevLett.77.3865.

[37] Andrae, D.; Huermann, U.; Dolg, M.; Stoll, H.; Preu, H. Energy-Adjustedab Initio Pseudopotentials for the Second and Third Row Transition Elements. *Theor Chim Acta* 1990, *77*, 123–141, doi:10.1007/BF01114537.

[38] Binkley, J.S.; Pople, J.A.; Hehre, W.J. Self-Consistent Molecular Orbital Methods. 21. Small Split-Valence Basis Sets for First-Row Elements. *J Am Chem Soc* 1980, *102*, 939–947, doi:10.1021/ja00523a008.

[39] Lazar, P.; Karlický, F.; Jurečka, P.; Kocman, M.; Otyepková, E.; Šafářová, K.; Otyepka, M. Adsorption of Small Organic Molecules on Graphene. *J Am Chem Soc* 2013, *135*, 6372–6377, doi:10.1021/ja403162r.

[40] Jansen, G. Symmetry-adapted Perturbation Theory Based on Density Functional Theory for Noncovalent Interactions. *WIREs Computational Molecular Science* 2014, *4*, 127–144, doi:10.1002/wcms.1164.

[41] Heßelmann, A.; Jansen, G.; Schütz, M. Density-Functional Theory-Symmetry-Adapted Intermolecular Perturbation Theory with Density Fitting: A New Efficient Method to Study Intermolecular Interaction Energies. *J Chem Phys* 2005, *122*, doi:10.1063/1.1824898.

[42] Adamo, C.; Barone, V. Toward Reliable Density Functional Methods without Adjustable Parameters: The PBE0 Model. *J Chem Phys* 1999, *110*, 6158–6170, doi:10.1063/1.478522.

[43] MOSZYNSKI, R. Symmetry-Adapted Perturbation Theory for the Calculation of Hartree-Fock Interaction Energies. *Mol Phys* 1996, *88*, 741–758, doi:10.1080/00268979650026262.

[44] Figgen, D.; Peterson, K.A.; Dolg, M.; Stoll, H. Energy-Consistent Pseudopotentials and Correlation Consistent Basis Sets for the 5d Elements Hf–Pt. *J Chem Phys* 2009, *130*, doi:10.1063/1.3119665.

[45] Kendall, R.A.; Dunning, T.H.; Harrison, R.J. Electron Affinities of the First-Row Atoms Revisited. Systematic Basis Sets and Wave Functions. *J Chem Phys* 1992, *96*, 6796–6806, doi:10.1063/1.462569.

[46] Řezáč, J.; Hobza, P. Extrapolation and Scaling of the DFT-SAPT Interaction Energies toward the Basis Set Limit. *J Chem Theory Comput* 2011, *7*, 685–689, doi:10.1021/ct200005p.

[47] Boys, S.F.; Bernardi, F. The Calculation of Small Molecular Interactions by the Differences of Separate Total Energies. Some Procedures with Reduced Errors. *Mol Phys* 1970, *19*, 553–566, doi:10.1080/00268977000101561.

[48] Frisch, M.J.; Trucks, W.; Schlegel, H.B.; Scuseria, G.E.; Robb, M.A.; Cheeseman, J.R.; Scalmani, G.; Barone, V.; Mennucci, B.; Petersson, G.A.; et al. *Gaussian 09, Revision B.01; Gaussian*; 2010; pp. 2009–2009;.

[49] Werner, H.J.; Knowles, P.J.; Knizia, G.; Manby, F.R.; Schütz, M. Molpro: A General-Purpose Quantum Chemistry Program Package. *Wiley Interdiscip Rev Comput Mol Sci* 2012, *2*, 242–253, doi:10.1002/wcms.82.

[50] Dennington, R.; Keith, T.; Millam, J. GaussView, Version 5. *Semichem Inc. , Shawnee Mission, KS* 2009, Semichem Inc.

[51] Munny, K.N.; Ahmed, T.; Piya, A.A.; Shamim, S.U.D. Exploring the Adsorption Performance of Doped Graphene Quantum Dots as Anticancer Drug Carriers for Cisplatin by DFT, PCM, and COSMO Approaches. *Struct Chem* 2023, *34*, 2089–2105, doi:10.1007/s11224-023-02150-y.

[52] Johnston, D.H.; Miller, N.A.; Tackett, C.B. Cis-Diamminedichloridoplatinum(II) N, N-Dimethylformamide Monosolvate. *Acta Crystallographica Section E* 2012, *68*, m863–m864, doi:10.1107/S1600536812024014.

[53] Zhou, X.; Zhao, C.; Wu, G.; Chen, J.; Li, Y. DFT Study on the Electronic Structure and Optical Properties of N, Al, and N-Al Doped Graphene. *Appl Surf Sci* 2018, *459*, 354–362, doi:10.1016/j.apsusc.2018.08.015.

[54] Yutomo, E.B.; Noor, F.A.; Winata, T. Effect of the Number of Nitrogen Dopants on the Electronic and Magnetic Properties of Graphitic and Pyridinic N-Doped Graphene – a Density-Functional Study. *RSC Adv* 2021, *11*, 18371–18380, doi:10.1039/D1RA01095F.

[55] Liu, J.; Liang, T.; Tu, R.; Lai, W.; Liu, Y. Redistribution of π and σ Electrons in Boron-Doped Graphene from DFT Investigation. *Appl Surf Sci* 2019, *481*, 344–352, doi:10.1016/j.apsusc.2019.03.109.

[56] Agnoli, S.; Favaro, M. Doping Graphene with Boron: A Review of Synthesis Methods, Physicochemical Characterization, and Emerging Applications. *J Mater Chem A Mater* 2016, *4*, 5002–5025, doi:10.1039/C5TA10599D.

[57] Ngidi, N.P.D.; Ollengo, M.A.; Nyamori, V.O. Tuning the Properties of Boron-Doped Reduced Graphene Oxide by Altering the Boron Content. *New Journal of Chemistry* 2020, *44*, 16864–16876, doi:10.1039/D0NJ03909H.